J Membrane Biol (2010) 235:131–143
DOI 10.1007/s00232-010-9264-3

Evaluation of a Two-Site, Three-Barrier Model for Permeation in $Ca_V3.1$ (α1G) T-Type Calcium Channels: Ca^{2+}, Ba^{2+}, Mg^{2+}, and Na^+

Kyle V. Lopin · Carlos A. Obejero-Paz · Stephen W. Jones

Received: 3 February 2010 / Accepted: 11 May 2010 / Published online: 29 May 2010

Abstract We explored the ability of a two-site, three-barrier (2S3B) Eyring model to describe recently reported data on current flow through open $Ca_V3.1$ T-type calcium channels, varying Ca^{2+} and Ba^{2+} over a wide range (100 nM–110 mM) while recording whole-cell currents over a wide voltage range (−150 mV to +100 mV) from channels stably expressed in HEK 293 cells. Effects on permeation were isolated using instantaneous current–voltage relationships (IIV) after strong, brief depolarizations to activate channels with minimal inactivation. Most experimental results were reproduced by a 2S3B model. The model described the IIV relationships, apparent affinities for permeation and block for Ca^{2+} and Ba^{2+}, and shifts in reversal potential between Ca^{2+} and Ba^{2+}. The fit to block by 1 mM Mg_i^{2+} was reasonable, but block by Mg_o^{2+} was described less well. Surprisingly, fits were comparable with strong ion–ion repulsion, with no repulsion, or with intermediate values. With weak repulsion, there was a single high-affinity site, with a low-affinity site near the cytoplasmic side of the pore. With strong repulsion, the net charge of ions in the pore was near +2 over a relatively wide range of concentration and voltage, suggesting a knockoff mechanism. With strong repulsion, Ba^{2+} preferred the inner site, while Ca^{2+} preferred the outer site, potentially explaining faster entry of Ni^{2+} and other pore blockers when Ba^{2+} is the charge carrier.

Keywords Eyring model · Rate theory · Channel block · Chord conductance · Ion selectivity · Patch clamp · Reversal potential

Paradoxically, understanding ion selectivity in calcium channels began with the recognition that a calcium channel is fundamentally a nonselective cation channel (Almers and McCleskey 1984; Almers et al. 1984; Hess and Tsien 1984; McCleskey and Almers 1985). In the absence of Ca_o^{2+}, calcium channels have a high conductance to monovalent cations. Initial models proposed two distinct binding sites, each of which could bind a single Ca^{2+} with high affinity (Almers and McCleskey 1984; Hess and Tsien 1984). That explained why monovalent ions carry current in the absence of Ca_o^{2+}, and why such currents are blocked by micromolar concentrations of Ca^{2+}. To explain permeation, the models assumed that electrostatic repulsion increases the rates of Ca^{2+} exit from the pore, when both sites are occupied by Ca^{2+}. Those pioneering models for calcium channel selectivity were based on Eyring rate theory, and included two binding sites and three barriers (2S3B), where one barrier is the transition state between the binding sites, and the others are for ion entry/exit.

Several theoretical and practical objections have been raised to the use of Eyring models for permeation in calcium channels. The preexponential factors have been criticized (Nonner et al. 1999), but this does not affect the actual calculation of rate constants (McCleskey 1999) (see also "Materials and Methods"). Previous calcium channel models predict significant changes in the net charge of all ion bound within the pore (as a function of voltage and concentration), while Poisson–Nernst–Planck calculations suggest a nearly electroneutral pore (Nonner and Eisenberg 1998). Eyring models often overpredict the nonlinearity of

Electronic supplementary material The online version of this article (doi:10.1007/s00232-010-9264-3) contains supplementary material, which is available to authorized users.

K. V. Lopin · C. A. Obejero-Paz · S. W. Jones (✉)
Department of Physiology and Biophysics, Case Western Reserve University, Cleveland, OH 44106, USA
e-mail: swj@case.edu

current–voltage (IV) relationships (Levitt 1986; Nonner et al. 1999). And mutational studies on L-type calcium channels demonstrate that high-affinity binding can be disrupted by single mutations within the pore, arguing against two physically separate ion binding sites (Yang et al. 1993).

One approach is to determine whether Eyring models, when strongly constrained by experimental data, provide physically realistic parameters: Let the data decide (Bergling 1999). We examine here whether a 2S3B model can describe permeation through a T-type calcium channel, under a wide range of ionic conditions (varying Ca^{2+} and Ba^{2+} from 10^{-7} to 0.11 M; varying extracellular and intracellular Mg^{2+}), and a wide voltage range (usually −150 mV to +100 mV) (Khan et al. 2008). The data set was based primarily on whole-cell recordings, but the use of instantaneous IV relationships (IIV) (Hodgkin and Huxley 1952) isolated effects on permeation from effects of voltage or ion concentration on channel gating. The data exhibited well-known features of calcium channel permeation, notably high conductance to Na^+ in the absence of divalent ions, block by Ca^{2+}, Ba^{2+}, and Mg^{2+}, and permeation at millimolar concentrations of Ca^{2+} and Ba^{2+}. Less standard features of our data set include complex, nonlinear IIVs, complex Ca^{2+} vs. Ba^{2+} selectivity (similar currents over a wide range of concentration and voltage, yet Ca^{2+} selectivity by the criteria of reversal potentials and sensitivity to Mg^{2+} block), and nearly voltage-independent apparent dissociation constants (K_D) for Ca^{2+} or Ba^{2+} permeation despite strongly voltage-dependent K_D values for block by those ions (Khan et al. 2008). This extensive data set is a stringent test for any model of calcium channel permeation.

We found that most, but not all, features of the data were described well by a 2S3B model. The primary discrepancies relate to block by Mg_o^{2+}. Our simulations demonstrate that ion–ion repulsion is not necessary to produce Ca^{2+} block (at μM concentrations) and Ca^{2+} permeation (at mM concentrations), although for our particular data set a model without repulsion did not accurately describe the time course of Ca^{2+} block. Furthermore, for models with weak ion–ion repulsion, only one of the two sites has to bind Ca^{2+} with high affinity.

Materials and Methods

The 2S3B model was based on Almers and McCleskey (1984). Rate constants were calculated as

$$k = k_o e^{-(z\delta VF+\Delta G)/RT}$$

where z is the charge on the ion, V is the membrane potential, ΔG is the difference in energy levels between a well and a barrier, and δ is the fraction of the electrical distance across the membrane between the well and barrier (outside = 0, inside = 1). When both sites were occupied, electrical repulsion between bound ions enhanced exit from the pore by a factor Q^{z1*z2} (where Q is a constant, and $z1$ and $z2$ are the charges on the two ions in the pore). Ion entry into an open site was not affected by occupancy of the other site (Almers and McCleskey 1984).

For comparison to most previous Eyring models, we use a preexponential factor $k_o = 6.1 \times 10^{12}$ s^{-1}, or for entry rates $k_o = C \times 6.1 \times 10^{12}$ $M^{-1}s^{-1}$, where C is the ion concentration in molar. Taken literally, this assumes that the fastest possible rate of ion entry at 1 M concentration equals the fastest possible rate of ion movement from site to site within the pore. That is physically unrealistic (Nonner et al. 1999), but if a different preexponential factor were chosen, the same rate constant can be produced by simply changing the energy barrier for all ion entry steps by a constant factor (McCleskey 1999). The appropriate factor depends on the maximal rate of ion entry via diffusion, which depends, for example, on the diameter of the pore. One study proposed that k_o should be multiplied by 0.00673, which is equivalent to lowering all of the energy levels in the model by 5.00 RT units (Yue and Marban 1990). Thus, the energies for ion entry should not be interpreted literally, since they exaggerate the barrier heights, but the rate constants are unaffected. That is sufficient for our purpose here, which is to calculate the rate of ion flow through the pore.

The experimental data were from Khan et al. (2008). Briefly, whole-cell recordings were made from HEK 293 cells stably transfected with rat $Ca_V3.1$ (α1G). Currents were evoked from a holding potential of −100 mV, or −120 mV in experiments with <0.5 mM Ca^{2+} or Ba^{2+}, to prevent resting inactivation. Channels were maximally activated (with minimal inactivation) by 2-ms depolarizations to +60 mV (Serrano et al. 2000), followed by voltage steps from +100 to −150 mV in 10 mV intervals (+100 to −120 mV in some conditions where currents were extremely large). Instantaneous current–voltage relationships (IIVs) were measured by fitting the initial portion of current decay (from peak, typically 0.2–0.5 ms, to 20 ms) to a single exponential. Voltages were corrected for junction potentials when >1 mV. Series resistance was compensated, usually by 80% or more. The average residual series resistance error after compensation was estimated to be 0.75 MΩ (producing 0.75 mV of voltage error per nA of current). No correction was made for this effect. IIV relations calculated in this manner isolate effects of ions and voltage on permeation from effects on gating. Effectively, the IIV relationships should be directly proportional to the single channel i–V relationship, simply multiplied by the average number of channels per cell. We estimated

the average number of channels per cell to be 8000, a value that gave a reasonable scaling factor between our whole-cell IIV relationships and available single-channel current measurements (see "Discussion").

24 data sets were included, with IIVs in 10 mV increments from −150 or −120 mV to +90 or +100 mV (Khan et al. 2008). The data are freely available in Excel spreadsheet form, as online supplementary material for Khan et al. (2008). For the dose–response relationships for Ca_o^{2+} and Ba_o^{2+}, $[Ca^{2+}]_o$ or $[Ba^{2+}]_o$ = 0.0001, 0.01, 0.1, 0.5, 2, 8, and 110 mM, with standard Mg_i^{2+} (1 mM calculated free Mg_i^{2+}) and 0 Mg_o^{2+}. For Mg_o^{2+} block, $[Mg^{2+}]_o$ = 0.3, 1, 3, and 10 mM (with 2 mM Ba_o^{2+}) and Mg_o^{2+} = 1, 3, 10, and 30 mM (with 2 mM Ca_o^{2+}), all with standard Mg_i^{2+}. Two data sets were included with pipet solutions containing no Mg_i^{2+} or ATP (100 nM Ca_o^{2+} and 2 mM Ca_o^{2+}). IIV relations were similar with a pipet solution containing MgATP but with Mg_i^{2+} buffered to 0.2 mM, suggesting that the effect depends on Mg_i^{2+} not $MgATP_i$ (Khan et al. 2008). Both extracellular and intracellular solutions contained 145 mM Na^+, reduced where extracellular divalent concentrations were 30 mM or higher (Khan et al. 2008).

Final parameter estimation was performed by MatLab with the function nlinfit using a Levenberg–Marquardt algorithm for nonlinear regression, modified to minimize the sum of absolute errors between the IIV data and the model calculations. Minimizing the sum of squared errors unduly emphasized the largest currents (which have the largest experimental error), which occasionally led to substantial errors in the estimated reversal potentials. State occupancies were calculated using matrix methods, and the current was calculated as the rate of net charge movement over the central barrier. 95% confidence intervals were found using the MatLab function nlparci using the Jacobian and residuals calculated by the Levenberg-Marquardt algorithm. There were 26 free parameters: 5 barrier or well energy levels × 4 ions, 5 electrical distances, and an ion–ion repulsion factor (Table 1). The parameter sets presented here are with the ion–ion repulsion factor fixed, to a range of different values. The barriers for ion entry were constrained to be >6 RT units, except for Ca^{2+} entry from the extracellular side, constrained to be >8 RT units (equivalent to an entry rate $<2 \times 10^9$ $M^{-1}s^{-1}$), given our data on the time course of block by 3–10 μM Ca^{2+}, as discussed further below.

We attempted to fit our data to a 3S4B model without ion–ion repulsion (Dang and McCleskey 1998), but were not able to obtain reliable parameter estimates, probably resulting from the increased number of free parameters.

Calculations were also performed by the SCoP simulation package version 3.52 (http://www.simresinc.com/), using numerical integration to calculate the steady-state occupancy of each state, and then the resulting fluxes. Fitting with the SCoPFit program gave similar results to MatLab (not shown), although three data sets had to be excluded (0.5 and 8 mM Ca^{2+}; 8 mM Ba^{2+}), and two others averaged (100 nM Ca^{2+} and 100 nM Ba^{2+}), because that program is limited to 20 data sets.

Another program, written in VisualBasic v. 6.0, was based on the analytic solution to state occupancy for the 2S3B model with two ions present. The three methods (MatLab, SCoP, and VisualBasic) calculated equivalent currents for a given parameter set. The VisualBasic program could also display a diagram of state occupancies, rate constants, and fluxes through each pathway for a given voltage and ionic condition, useful for developing intuition regarding the inner workings of the model.

The current through an open calcium channel changes instantaneously upon step changes in voltage, except at low (1–10 μM) Ca_o^{2+}, where time-and voltage-dependent block by Ca^{2+} introduces fast time-dependent relaxations (Khan et al. 2008). Time-dependent block was evaluated in two ways. First, a program (written in VisualBasic) calculated the currents resulting from stochastic transitions of ions among channel states, based on the 2S3B model. This simulates single-channel currents. Briefly, given an initial channel state, one pseudorandom number determines

Table 1 Parameters for 2S3B permeation model[a] with $Q = 5$

Site	Electrical distance	Barrier/well energies (RT)			
		Ca^{2+}	Ba^{2+}	Mg^{2+}	Na^+
Outer barrier	0.095 ± 0.032	8.12 ± 0.61	8.74 ± 0.62	10.47 ± 1.20	10.99 ± 0.37
Outer well	0.501 ± 0.033	−13.45 ± 0.53	−12.82 ± 0.51	−9.62 ± 1.05	−2.00 ± 0.63
Central barrier	0.553 ± 0.043	0.96 ± 0.76	1.46 ± 0.85	9.68 ± 0.79	6.49 ± 16.06
Inner well	0.644 ± 0.046	−11.25 ± 0.31	−11.19 ± 0.28	−6.44 ± 1.07	−2.90 ± 0.54
Inner barrier	0.999 ± 0.062	10.64 ± 0.37	11.02 ± 0.40	6.30 ± 1.28	10.16 ± 0.73

[a] Parameters were estimated for the Almers and McCleskey (1984) model as described in "Materials and Methods". The ion–ion repulsion factor (Q) was fixed to 5. See middle column in Figs. 1–2. Error bars are the 95% confidence intervals (maximum or minimum) minus the mean. Positive and negative errors were symmetrical. Note that the central barrier for Na^+ was not well constrained

which of the allowed transitions occurs (weighted by the rate constants for each transition), and a second pseudo-random number determines the time to the next transition (by sampling an exponential distribution with time constant = the reciprocal of the sum of all rate constants leading away from the current state). This method (Gillespie 1977) has also been used, for example, for stochastic channel gating models (Chow and White 1996). For the parameters sets with $Q = 1$ or $Q = 11.89$ (Supplementary Tables 2 and 3), one step (movement of Na^+ over the central barrier) was extremely fast, but was not rate limiting for current flow, so the central barrier was adjusted (to +4.0 or +8.0, respectively), which did not markedly affect the deterministically calculated currents. Second, MatLab was used to calculate the time-resolved response to a voltage step (from +60 mV to the desired voltage, as for the experimentally used IIV protocol). This simulates the fast component of tail currents seen with low Ca_o^{2+} (Khan et al. 2008).

Results

Effect of Ion–Ion Repulsion

Electrostatic repulsion between ions at high-affinity binding sites within the pore was fundamental to the initial explanation of Ca^{2+} permeation using 2S3B models (Almers and McCleskey 1984; Hess and Tsien 1984). So we were surprised to find that a wide range of ion–ion repulsion factors (Q) can account for the main qualitative features of Ca^{2+} channel permeation. This does not mean that Q is not important, as Q strongly affects the other parameters of the model, and indeed the mechanisms of Ca^{2+} permeation and selectivity. Figure 1 compares three parameter sets, with no ion–ion repulsion at all ($Q = 1$), with our best overall fit ($Q = 5$), and with $Q = 11.89$ (as in Almers and McCleskey 1984). Parameters are given in Table 1 and in Supplementary Tables 1 and 2. Features common to all three parameter sets are similar energy profiles for Ca^{2+} and Ba^{2+}, a high central barrier for Mg^{2+} (explaining its blocking action), and weak binding of Na^+ to both sites (Fig. 1a). However, the models differ in other key respects.

With $Q = 1$, the outer well is considerably deeper for Ca^{2+} and Ba^{2+}, effectively producing one high affinity site flanked by a low affinity site. A Ca^{2+} ion at the high affinity site can permeate by two relatively small steps, rather than one large leap. This is reminiscent of the 3S4B model of Dang and McCleskey (1998), but apparently the outer low affinity site in that model is not necessary. In mixtures of Ca^{2+} and Na^+, Ca^{2+} permeation usually requires double occupancy of the pore by Ca^{2+}, reflected in a large variation in the summed charge of all ions in the pore as a function of concentration and voltage (Fig. 1b, left). That is, saturation of Ca^{2+} current through the channel parallels saturation of the second binding site with Ca^{2+} ions. The energy wells are slightly deeper for Ca^{2+} vs. Ba^{2+}, but the inner barrier for Ca^{2+} is slightly lower, explaining the paradox that T channels are selective for Ca^{2+} over Ba^{2+} by the criterion of reversal potential (reflecting binding), but Ca^{2+} and Ba^{2+} currents are closely similar.

In contrast, with $Q = 11.89$, there clearly are two high affinity sites near the middle of the pore (Fig. 1a, right). At most Ca^{2+} concentrations and voltages, the summed charge of all ions in the pore is approximately 2 (Fig. 1b, right). Most of the time, there is a single Ca^{2+} ion in the pore, and entry of a second Ca^{2+} ion rapidly expels the first into the cytoplasm, a knockoff mechanism. For this model, Ca^{2+} prefers the outer site while Ba^{2+} prefers the inner site (Fig. 1c), not true for $Q = 1$.

The model with mild electrostatic repulsion ($Q = 5$) uses a hybrid mechanism for selectivity. The outer energy well is lower than the inner well for Ca^{2+} and Ba^{2+}, but not by as large an amount as with $Q = 1$ (Fig. 1a). The net ionic charge in the pore is closer to 2 than with $Q = 1$, but there is more variation than with $Q = 11.89$ (Fig. 1b). The difference in preference of Ca^{2+} vs. Ba^{2+} for inner vs. outer sites is also intermediate (Fig. 1c).

The parameter set with $Q = 5$ was the best fit overall to the IIV relationships. However, the error in the fit was only 1% higher with $Q = 11.89$. Indeed, the error was only 1–11% higher for the best fit parameters with Q fixed to 2–1000 (not shown). With $Q = 1$, the error was considerably higher (48%), so we conclude that our particular data set cannot be quantitatively described by a 2S3B model without incorporating some degree of ion–ion repulsion. However, if we allow somewhat more rapid influx of extracellular Ca^{2+} (outer barrier $\sim$6 RT), the error with $Q = 1$ was only 5% higher than with $Q = 5$ (parameters given in Supplementary Table 3).

Time-Dependent Block by Ca_o^{2+}

The time course of Ca_o^{2+} block of current carried by Na^+ through T channels can be observed either as fast relaxations in whole-cell currents, or as fast transitions at the single-channel level (Khan et al. 2008; Lux et al. 1990). Our estimate of the channel blocking rate, depending on the method used, was 2–6 $\times$ 10^8 $M^{-1}s^{-1}$, near the diffusion limit (Khan et al. 2008). Therefore, we wanted to determine whether the models truly reproduce time-dependent block.

First, we simulated single-channel behavior using a stochastic version of the 2S3B model, where ions were

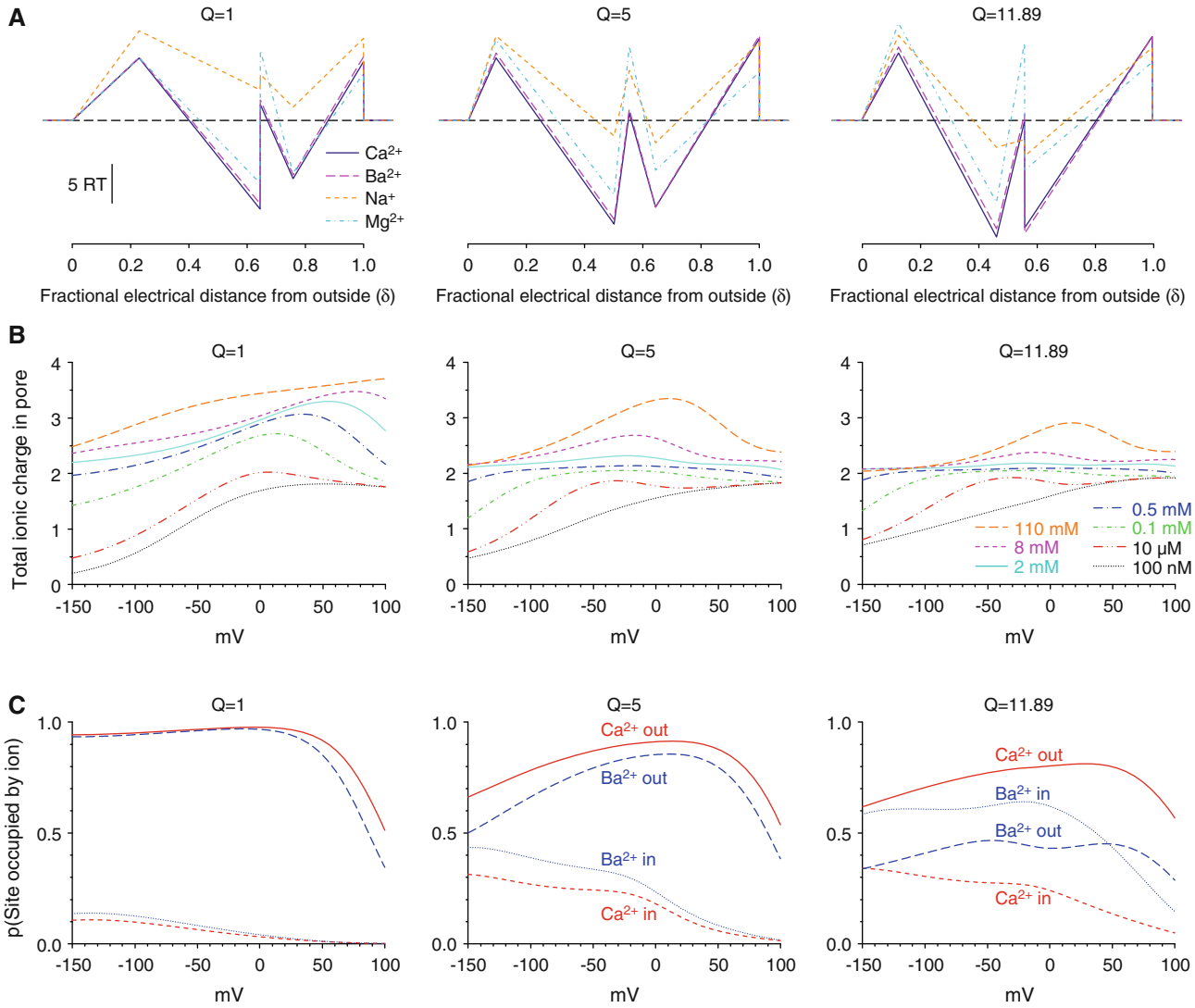

Fig. 1 Models for permeation and block, based on Almers and McCleskey (1984), as described in "Materials and Methods". **a** Energy level diagrams for Ca^{2+}, Ba^{2+}, Mg^{2+}, and Na^{+}. Assuming a preexponential factor of 6.1×10^{12} for all rate constants (including ion entry into the pore), an energy of 5 RT corresponds to a rate constant representation (RCR) of 3.15 (Andersen 1999). Parameters are the best fits obtained for three values of the ion–ion repulsion factor (Q), with numerical values in Table 1 ($Q = 5$) and Supplementary Tables 1 and 2 ($Q = 1$, $Q = 11.89$). The energy profiles are for a single channel, fitted assuming that experimental macroscopic currents result from 8000 channels per cell. **b** The predictions of the two-site, three-barrier (2S3B) Eyring model for the total charge of all ions in the pore, calculated for the Ca_o^{2+} concentrations examined experimentally. **c** Probability of occupancy of outer vs. inner binding sites by Ca^{2+} or Ba^{2+}, calculated for 2 mM Ca_o^{2+} or 2 mM Ba_o^{2+}

allowed to randomly move in and out of the channel (and between the two binding sites within the channel) according to the rate constants calculated from the fitted parameters (see "Materials and Methods"). Figure 2 shows simulated channel block with 3 μM Ca_o^{2+} at −70 mV. The current integrated at 10-μs intervals revealed very rapid blocking and unblocking events *(upper records)*. When filtered at 2 kHz (to simulate the filtering used experimentally), it is clear that many events were only partially resolved. For the parameter set with $Q = 1$, block is so rapid that there is only a decrease in the apparent single channel current, with individual blocking events unresolved. With higher Q, the rapid, flickery behavior qualitatively resembles the experimentally observed channel gating in 3 μM Ca_o^{2+} (Khan et al. 2008). Quantitatively, with $Q = 5$, the mean open time (measured by standard 50% amplitude crossing) is 0.15 ms at 100 kHz resolution, but 0.47 ms at 2 kHz. The latter value agrees well with the experimental open time of 0.64 ms (corrected assuming that the observed mean open time of 0.85 ms in 0.1 μM Ca_o^{2+} reflects the normal channel closing rate, and that closing and block are independent) (Khan et al. 2008).

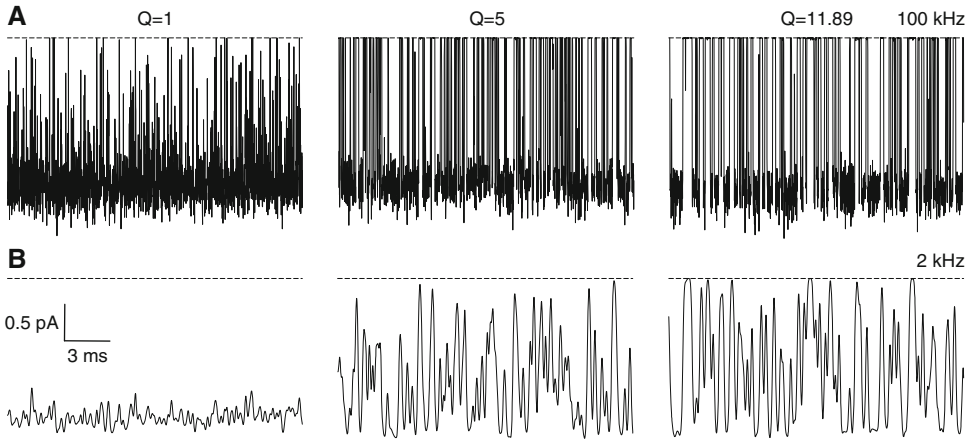

Fig. 2 Simulated block by 3 μM Ca_o^{2+} of currents carried by Na^+, at −70 mV, for the same three parameter sets as in Fig. 1. The *upper records* show the calculated current, with each point being the integrated current over a 10 μs interval. The *lower records* show the same simulations after digital Gaussian filtering at 2 kHz. Zero current is indicated with *dashed lines*. Same time and current scale for all records. Compare to Fig. 8A of Khan et al. (2008), noting that experimentally observed burst durations are limited by the mean open time of ~0.8 ms in the absence of Ca_o^{2+}

Next, we calculated the expected whole-cell current relaxation resulting from block by 3 μM Ca_o^{2+} at −50 mV (see "Materials and Methods"). The time constant was 0.05 ms with $Q = 5$ and 0.08 ms with $Q = 11.89$, compared to 0.53 ms experimentally (Khan et al. 2008). The experimentally observed relaxation will be slowed by series resistance error and filtering, but that may not fully account for the discrepancy. At any rate, it is clear that the model does predict a submillisecond relaxation in the macroscopic current resulting from Ca_o^{2+} block, as observed experimentally.

Effect of Ca_o^{2+} and Ba_o^{2+}

In summary, given our experimental data, we can exclude $Q = 1$, while $Q = 5$ and $Q = 11.89$ remain plausible. The remainder of the Results section presents simulations with the best fit parameter set ($Q = 5$).

Figure 3 shows a fit of the 2S3B model to experimental IIV relationships recorded in 100 nM to 110 mM Ca_o^{2+} or Ba_o^{2+}. In 100 nM Ca_o^{2+} or Ba_o^{2+}, currents are carried by Na^+, and the IIV relationship is nearly linear for inward currents, with weak rectification for outward currents, resulting from block by Mg_i^{2+} (Khan et al. 2008; discussed further below). Currents carried by Na^+ were progressively blocked by addition of 0.01–0.5 mM Ca^{2+} (Fig. 3a) or Ba^{2+} (Fig. 3c). At higher concentrations, inward currents increased with Ca^{2+} (Fig. 3b) or Ba^{2+} (Fig. 3d), reflecting currents carried by those ions, while outward Na^+ currents were blocked further. The model reproduced these qualitative features of the data, and provided a reasonably good quantitative description. Note that currents were only subtly different between Ca^{2+} vs. Ba^{2+} (Fig. 3).

However, increases in Ca^{2+} vs. Ba^{2+} differentially shifted the reversal potential (V_R). The symbols in Fig. 4 are V_R calculated from the 2S3B model for Ca^{2+} and Ba^{2+}. The concentration dependence of V_R was described well by Goldman-Hodgkin-Katz (GHK) theory (curves, Fig. 4), with subtle deviations in the 0.1–0.5 mM range. The best-fit GHK permeability ratios were $P_{Ca}/P_{Na} = 111$ (solid curve), and $P_{Ba}/P_{Na} = 67$ (dashed curve). Those values compare reasonably well to the experimental values ($P_{Ca}/P_{Na} = 87$ and $P_{Ba}/P_{Na} = 44$) (Khan et al. 2008).

These results are consistent with the classical view that calcium channels are intrinsically highly conductive to Na^+, but low concentrations of Ca^{2+} (and Ba^{2+}) block, while high (mM) concentrations result in inward currents carried by Ca^{2+} or Ba^{2+}. In addition, it is apparent that the strength of block, and the transition from block to permeation, depends on voltage as well as on concentration (Fig. 3). However, direct comparison of currents recorded at different voltages is complicated by changes in driving force, resulting from changes in V_R. This can be avoided by calculation of chord conductances (Fig. 5a, b and d, e). Since block is negligible at 100 nM Ca^{2+} or Ba^{2+} for the 2S3B model, the voltage-dependence of block can be calculated from chord conductance ratios (Fig. 5c, f). The 2S3B model again captures the main qualitative features, notably the U-shaped voltage-dependence (i.e., block is relieved either by strong depolarization or by strong hyperpolarization). Quantitative discrepancies, especially at the lower concentrations, result primarily from ~20% larger currents recorded experimentally in 100 nM Ba^{2+} vs. 100 nM Ca^{2+} for this data set (see Figs. 3a, c, 5a, d). Note that the data and 2S3B model both indicate slightly weaker block by 10 μM Ba^{2+}, compared to Ca^{2+}.

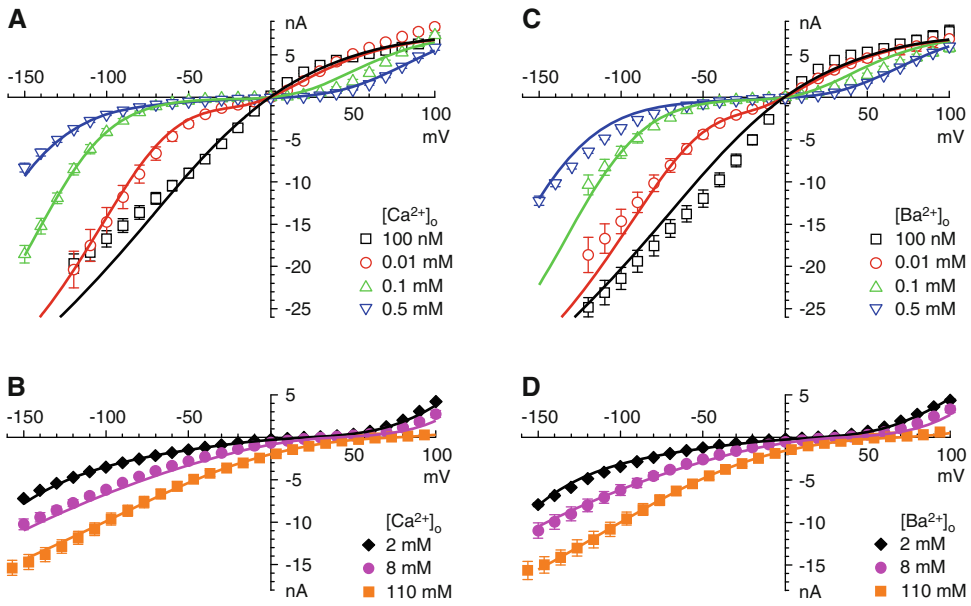

Fig. 3 IIV relationships. *Symbols* are the experimental data (Fig. 2 of Khan et al. 2008), and *solid curves* are the currents calculated from the two-site, three-barrier (2S3B) Eyring model

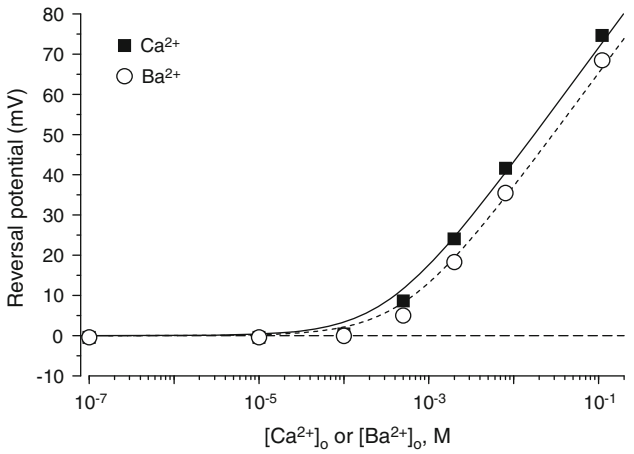

Fig. 4 Reversal potentials calculated from the two-site, three-barrier (2S3B) Eyring model. V_R was interpolated from IIV relations (Fig. 3) calculated in 1 mV intervals, for the indicated concentrations of Ca^{2+} and Ba^{2+}. *Symbols* are V_R values from the 2S3B model; *curves* are the best fit to GHK theory. Note that the *symbols* in this figure are not experimental data. Compare to Fig. 3 of Khan et al. (2008)

The voltage and current dependence of permeation and block were evaluated by fitting the conductance-concentration relationship to a simple empirical model, the sum of a conductance to Na^+ (G_{Na}, with voltage-dependent block by Ca^{2+} or Ba^{2+} reflecting saturable binding to a single site according to mass action) plus a conductance to Ca^{2+} or Ba^{2+} (reflecting occupancy of a single voltage-dependent binding site), as described by Khan et al. (2008). The fit is shown for representative voltages in Fig. 6a–d. Chord conductances calculated from the 2S3B model (symbols) were described well. Note that the decrease in current at lower concentrations was clearly voltage-dependent, strongest near −30 mV.

The conductances and apparent dissociation constants (K_D) are shown as a function of voltage in Fig. 6e, f. Here, symbols are the experimental values, and the curves are the values from analyzing the 2S3B simulated data in the same manner. With depolarization, G_{Na} decreased weakly, while G_{Ca} (or G_{Ba}) decreased more strongly but did not reach zero (Fig. 6e). The 2S3B model reproduced the strong U-shaped voltage dependence of block, but the K_D for permeation was ~2 mM with little voltage dependence.

Effect of Mg_o^{2+}

The 2S3B model described block by Mg_o^{2+} much less well (Fig. 7). The fit to the IIV relationships appeared reasonable for Ba^{2+}, but block was clearly overestimated in Ca^{2+} (Fig. 7a, d). Analyzed as chord conductances, the voltage dependence of block was not well described (Fig. 7b, e). The discrepancies are even more obvious in plots of the fractional block (Fig. 7c, f), where the 2S3B model produced a complex voltage dependence, deviating strongly from the data. Actually, a simple Woodhull model provided a more accurate description (dashed lines, Fig. 7c, f), but still exhibited subtle systematic deviations from the data (Khan et al. 2008). With the 2S3B model, Mg_o^{2+} block was stronger in Ba_o^{2+} vs. Ca_o^{2+}, but the difference was less than observed experimentally.

Effect of Mg_i^{2+}

The intracellular (pipet) solution for whole-cell recording typically includes MgATP, which results in significant free Mg_i^{2+} (1 mM in our experiments). Reduction of Mg_i^{2+} led to larger outward currents, nearly linearizing the IIV

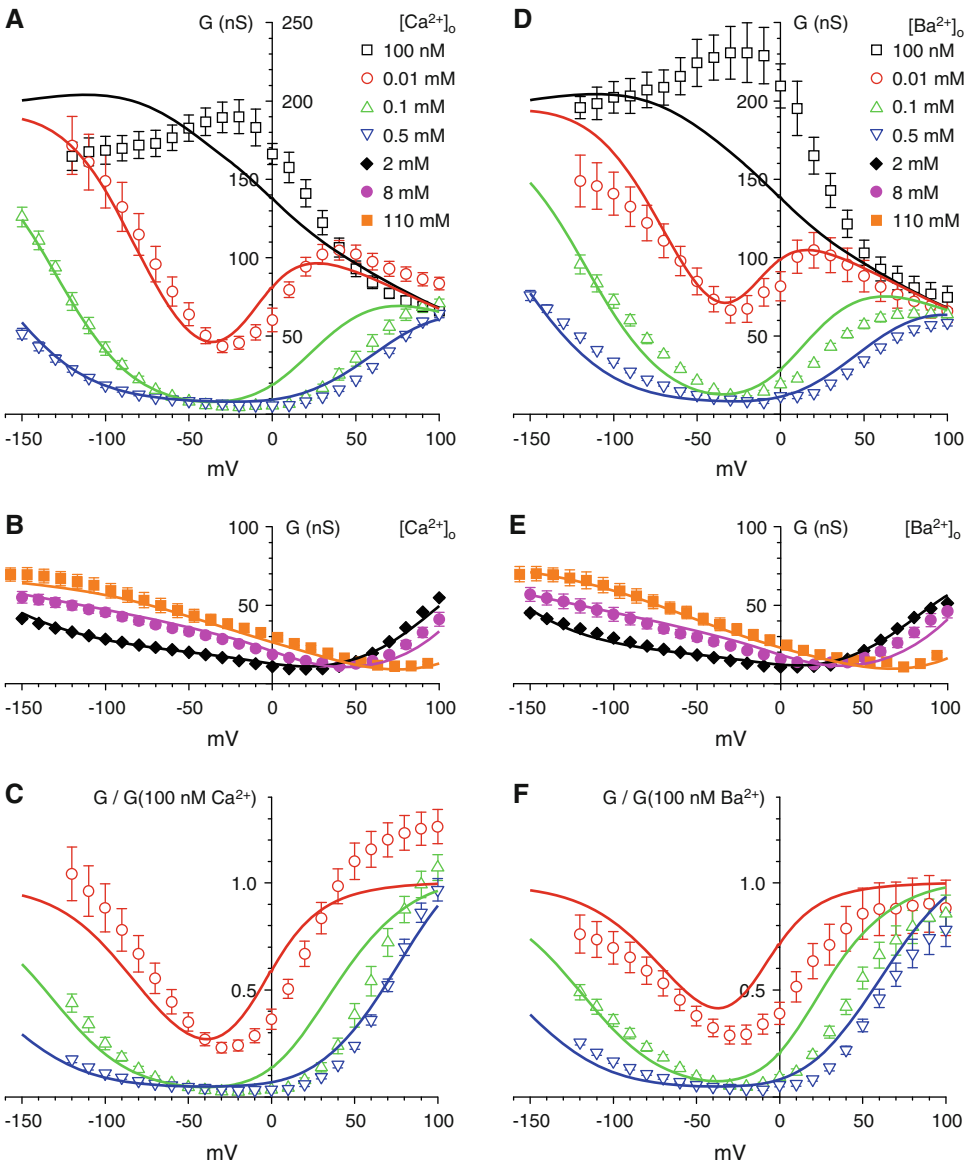

Fig. 5 Conductance–voltage relationships. Chord conductances were calculated from the IIV relationships in Fig. 3, for experimental values (*symbols*), and two-site, three-barrier (2S3B) Eyring model (*solid curves*). Compare to Fig. 4 of Khan et al. (2008)

relationship with Na^+ as the charge carrier, resulting from voltage-dependent block by Mg_i^{2+} (Khan et al. 2008). Block by Mg_i^{2+} was described reasonably well by the 2S3B model (Fig. 8).

Discussion

How Well Does the 2S3B Model Fit the Data?

A 2S3B Eyring model described selectivity of $Ca_V3.1$ among Ca^{2+}, Ba^{2+}, and Na^+ over a wide range of concentration and voltage, although the fit to Mg_o^{2+} block was less satisfactory. Notable features that the model described well include the overall shape of IIV relations over a very wide range of Ca_o^{2+} and Ba_o^{2+} (Fig. 3), the effects of Ca_o^{2+} and Ba_o^{2+} on V_R (including the more positive V_R with Ca_o^{2+}; Fig. 4), the dramatic difference in voltage-dependence of K_D for permeation vs. block (Fig. 6f), block by Mg_i^{2+} (Fig. 8), and time-dependent block by ~3 μM Ca_o^{2+} (Fig. 2). It is noteworthy that our 2S3B model can generate a wide range of IIV shapes, ranging from nearly linear (with 100 nM Ca_o^{2+}) to highly nonlinear (0.1–0.5 mM Ca_o^{2+} or Ba_o^{2+}). However, the model produced unnecessarily complex IIVs for Mg_o^{2+} block, especially visible when converted to chord conductances or fractional block (Fig. 7). We conclude that this model is not a complete description of permeation in $Ca_V3.1$, but it does reproduce many quantitative and qualitative features of the data.

The experimental data (whole-cell IIV relationships) should equal the single-channel current times the number of channels per cell. Assuming 8000 channels per cell, the

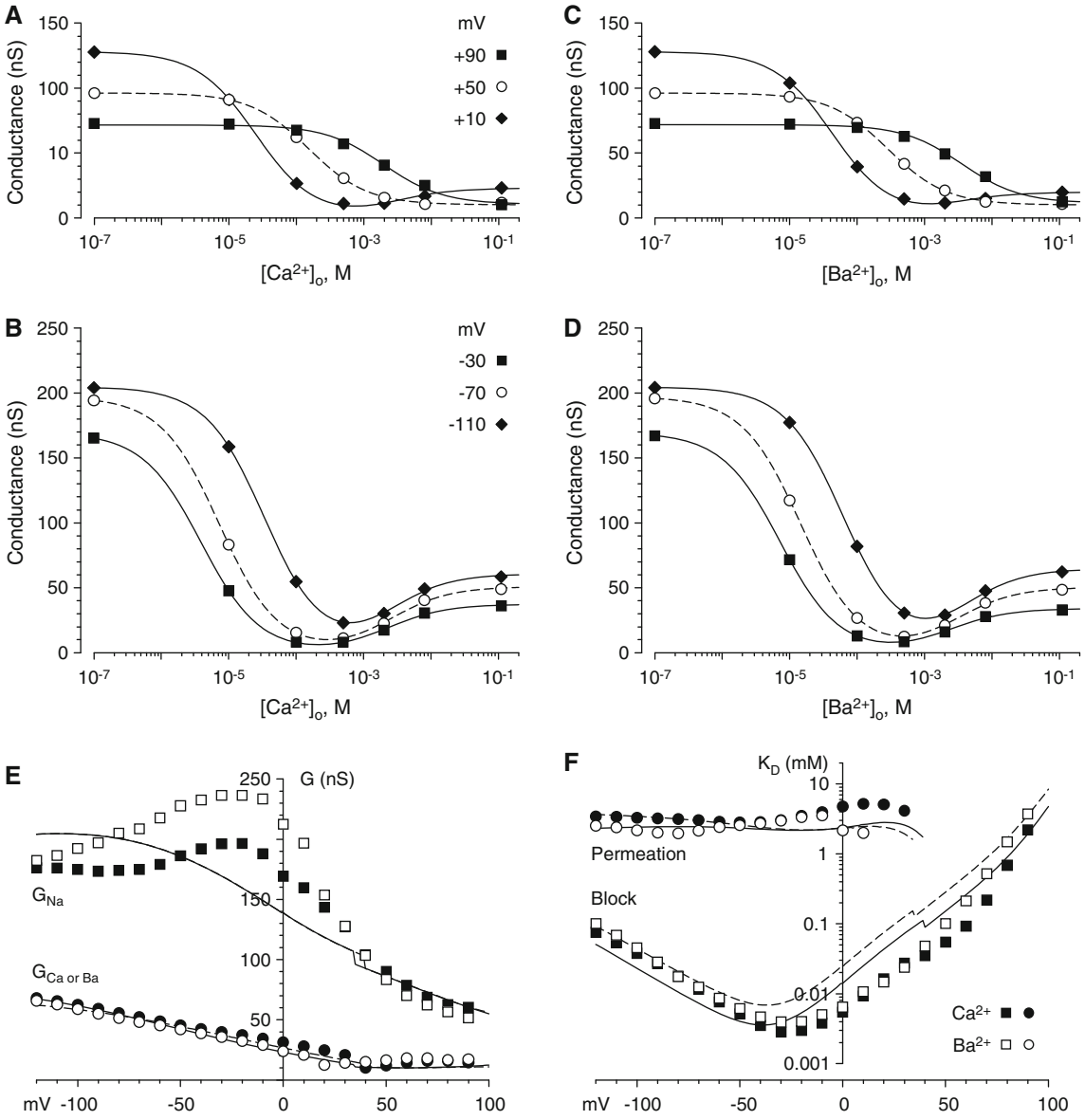

Fig. 6 Concentration- and voltage-dependence of block and permeation. **a**–**d** Chord conductances vs. $[Ca^{2+}]_o$ or $[Ba^{2+}]_o$, for the indicated voltages. The *symbols* are chord conductances calculated from the two-site, three-barrier (2S3B) Eyring model (theoretical curves in Fig. 5a, b, d, e), for the Ca^{2+} and Ba^{2+} concentrations used experimentally. The curves are fits to the sum of independent components for block (of current carried by Na^+) and permeation (see text and Eq. 4 of Khan et al. 2008). Parameters (G_{Na}, G_{Ca} or G_{Ba}, and apparent K_D values for block and permeation) were estimated by minimizing the sum of squared errors using the Solver function in Microsoft Excel. The *symbols* defined in **a** and **b** also apply to **c** and **d**, respectively. **e**, **f** Voltage dependence of conductances and apparent K_D values. *Symbols* are experimental values (Khan et al. 2008), and the *curves* are calculated from the 2S3B model. Parameters (G's and K_D's) were estimated separately for each voltage, as shown for representative voltages in **a**–**d**. *Solid curves* are for Ca_o^{2+}, *dashed curves* for Ba_o^{2+}. From +40 to +100 mV, the model conductances were described by the sum of a constant permeation term (with no K_D) and a blocking term (note slight discontinuity in the curves). Compare to Fig. 5 of Khan et al. (2008)

2S3B model predicted a slope conductance of 28 pS for current carried by Na_o^+ (−90 to −40 mV), compared to the experimental value of 33 pS (recorded with 105 mM Na_o^+, and K_i^+; Khan et al. 2008). The model's slope conductance was 11 pS in 110 mM Ca_o^{2+} and 12 pS in 110 mM Ba_o^{2+} (−50 to −10 mV), comparable to experimental values: 7.5 pS in Ba^{2+} (Perez-Reyes et al. 1998), or 9.5 pS in Ca^{2+} and 10.3 pS in Ba^{2+} (Bittner and Hanck 2008). As we noted previously (Khan et al. 2008), the commonly reported slope conductance is problematic as a measure of Ca^{2+} channel permeation, as it does not reflect the reversal potential. For example, the actual *currents* were 10–20% lower in 110 mM Ba^{2+} than in 110 mM Ca^{2+}, even though the *slope* was 10% larger in Ba^{2+}.

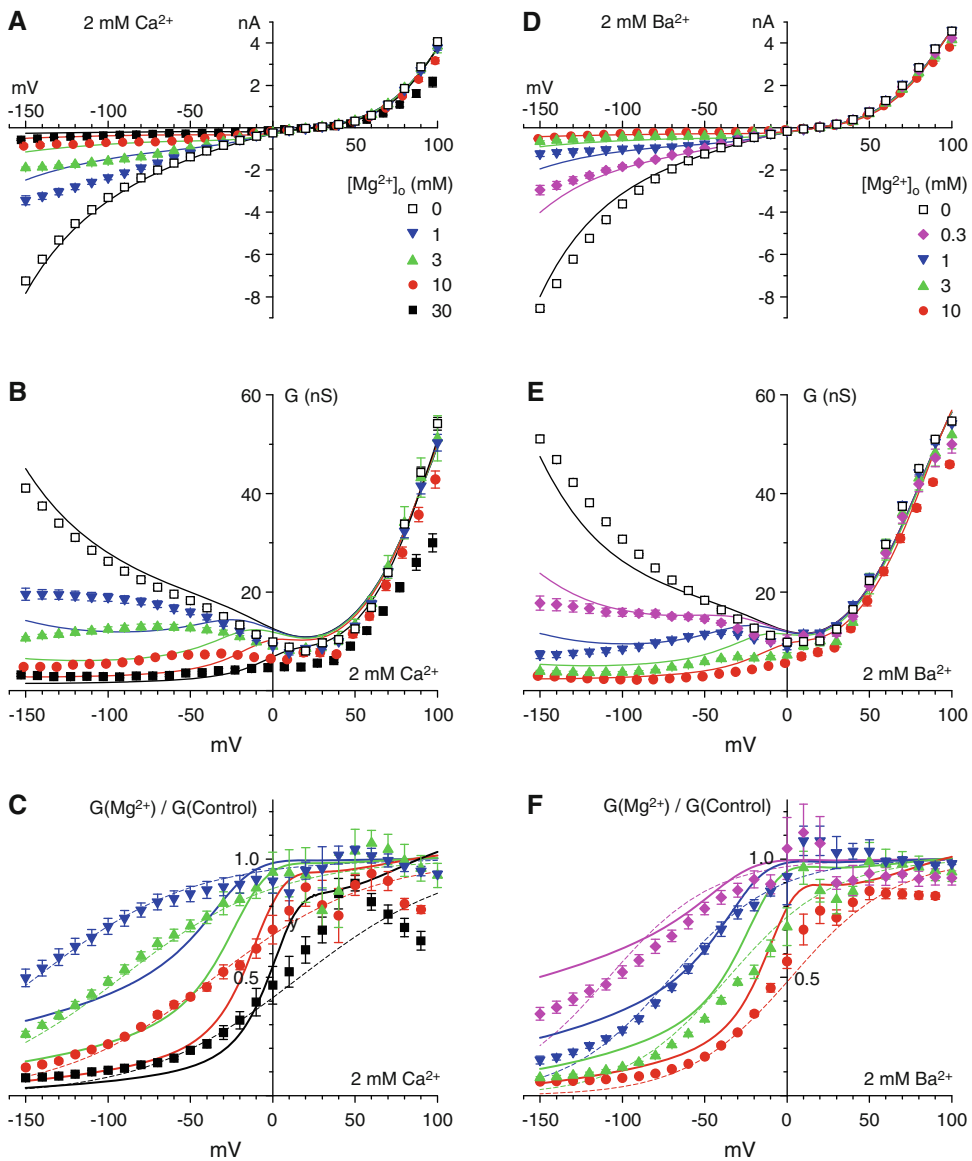

Fig. 7 Block by Mg_o^{2+}, with 2 mM Ca_o^{2+} (**a**–**c**) or 2 mM Ba_o^{2+} (**d**–**f**). *Symbols* are experimental values (Fig. S12A–D; Khan et al. 2008), and the *solid curves* are the corresponding values calculated from the two-site, three-barrier (2S3B) Eyring model. The effect of Mg_o^{2+} is shown as IIV relationships (**a**, **d**), chord conductances (**b**, **e**), and as conductance ratios (**c**, **f**). The *dashed lines* in **c** and **f** are fits to the experimental data assuming voltage-dependent block by Mg_o^{2+}, with no Mg^{2+} permeation (Woodhull 1973), from Fig. S12E,F of Khan et al. (2008)

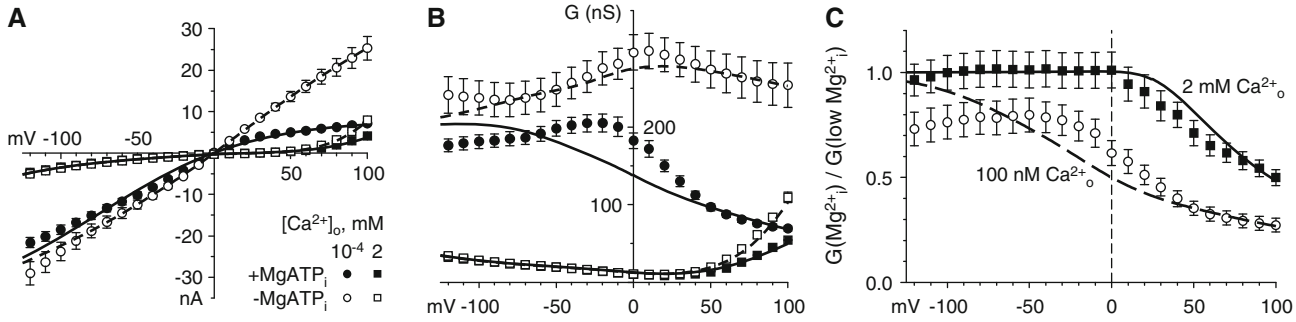

Fig. 8 Block by Mg_i^{2+}. *Symbols* are the experimental data (Fig. S19 of Khan et al. 2008) and *curves* are two-site, three-barrier (2S3B) Eyring model calculations, comparing cells with 1 mM $MgATP_i$ (*solid curves*) vs. 0–0.2 mM $MgATP_i$ (*dashed curves*). The 10^{-4} mM Ca^{2+} data actually include cells recorded in either 100 nM Ca^{2+} or 100 nM Ba^{2+} (n = 8, for both normal and low $MgATP_i$). Currents (**a**) and chord conductances (**b**). *Symbols* in **a** also apply to **b**. **c** Mg_i^{2+} block, calculated as chord conductance ratios, from the data and simulations in **a** and **b**

The model predicted a very small anomalous mole fraction effect between Ca_o^{2+} and Ba_o^{2+}, maximally a $\sim$1% decrease in current (compared to the smaller of the two currents calculated for Ca_o^{2+} or Ba_o^{2+} alone) at -140 mV for a Ca_o^{2+} mole fraction of 0.34 with 2 mM total $Ca_o^{2+} + Ba_o^{2+}$.

For this model, a small fraction of the inward current is carried by Na^+ in the presence of 2 mM Ca_o^{2+} (1% at -50 mV, 6% at -100 mV, 24% at -150 mV), and removal of Na_o^+ shifted V_R by -3.2 mV. This is consistent with our data, but the contribution of Na^+ entry was difficult to resolve experimentally since impermeant cations (e.g., N-methyl-D-glucamine) seem to block calcium channels (Khan et al. 2008; Kuo and Hess 1992).

Also consistent with our data, the model predicts negligible changes in V_R upon addition of Mg_o^{2+}. For example, 10 mM Mg_o^{2+} shifted V_R by +0.5 mV in 2 mM Ca_o^{2+} and +0.4 mV in 2 mM Ba_o^{2+}.

Our experimental data set did not examine effects of varying Na^+, but our model qualitatively reproduced effects of varying Na^+ on lymphocyte T channels (Yamashita et al. 1990) (simulations not shown). Specifically, changes in Na_o^+ have little effect (in the presence of Ca_o^{2+}), but changes in Na_i^+ strongly shift V_R, and change the amplitudes of outward currents at positive potentials. The supralinear increase in outward currents with Na_i^+, measured at +65 mV (Fig. 7 of Yamashita et al. 1990), is subtly visible with chord conductances, but results primarily from the change in driving force. Our model does allow double occupancy of the pore by Na^+ ions, but the calculated probability is low (<1% with 2 mM Ca_o^{2+}). It seems that constraining the IIV relationships with constant 145 mM Na^+ (but with varied Ca^{2+}, Ba^{2+}, and Mg^{2+}) was sufficient to describe Na^+ permeation.

Inner Workings of the 2S3B Model

To our knowledge, this study is the first attempt to fit a 2S3B model using automated parameter estimation procedures, with a data set sufficiently extensive to strongly constrain most of the model parameters. Serrano et al. (2000) used automated parameter estimation, but for a more limited data set (Mg_o^{2+} block at 1–2 concentrations, with 2 mM Ca_o^{2+} or Ba_o^{2+}). The parameters from that model do not describe well the full Ca_o^{2+} or Ba_o^{2+} concentration dependence, as might be expected.

We were surprised to find that the 2S3B model could fit the IIV relationships with essentially any value of Q, the ion–ion repulsion factor. For our data, we can exclude $Q = 1$, as the flickery block by Ca^{2+} of current carried by Na^+ was not described (Fig. 2). However, it is interesting as a theoretical point that a 2S3B model does not absolutely need ion–ion repulsion to explain key features of calcium channel permeation.

For all parameter sets considered here, the middle portion of the energy profile for Na^+ is not well defined (Table 1; Supplementary Tables 1–3). It appears that the data can be described well as long as Na^+ binding is weak, and movement of Na^+ between the two binding sites is not rate-limiting. Other parameters appear to be well constrained (for a given Q value).

For an Eyring permeation model, at a given voltage and set of concentrations, the calculated current depends both on the rate constants, and on the steady-state probability of observing each state of ion occupancy. It is noteworthy that the total charge of all ions bound within the channel can be relatively constant (Fig. 1b), even though the chemical identity of the ions in the pore varies substantially. This implies that saturation of Ca^{2+} current through the calcium channel does not require full occupancy by Ca^{2+} of both sites in the pore ($z = 4$). For high Q values, the rate-limiting step for Ca^{2+} influx at high concentrations is the rate of Ca^{2+} movement from the outer to the inner binding site (analysis not shown). This amounts to a knockoff mechanism for permeation, where entry of a second ion rapidly pushes the first ion into the cytoplasm, without need for a high steady-state probability of double occupancy. This contrasts with the Hess and Tsien (1984) model, proposed for L-type calcium channels (simulations not shown). That 2S3B model predicts very substantial changes in net pore occupancy, $z = 0.6$ at 100 nM Ca^{2+} (mostly Na^+), $z = 2$ at 0.1 mM Ca^{2+} (1 Ca^{2+} ion in pore), and $z = 4$ at 110 mM Ca^{2+} (2 Ca^{2+} ions in pore). For that model, saturation of Ca^{2+} current through the pore parallels saturation of Ca^{2+} occupancy. Ion occupancy in the Almers and McCleskey (1984) model is closer to our situation with $Q = 5$ or $Q = 11.89$.

The summed charge of $\sim$+2 for models with high Q is intriguing, given the -4 charge of the glutamates and aspartates at the presumed selectivity filter of a $Ca_V3.1$ pore. It is possible that nearby ions in the inner and/or outer vestibules (not considered in a 2S3B model) make the net charge in the pore closer to zero at any given time, as expected from Poisson–Nernst–Planck theory (Nonner and Eisenberg 1998).

How does the 2S3B model describe the differences (and similarities) between Ca^{2+} and Ba^{2+}? At first glance, the energy profiles are quite similar (Fig. 1). For $Q = 5$ or $Q = 11.89$, one striking difference is that Ba^{2+} prefers the inner site while Ca^{2+} prefers the outer site (Fig. 1c; note difference in energy wells, Fig. 1a). That may explain the higher entry rate of some blocking ions into Ba^{2+}-occupied pores (Obejero-Paz et al. 2004, 2008), as well as the more positive V_R (Fig. 4) and weaker block by Mg_o^{2+} with Ca_o^{2+} vs. Ba_o^{2+} (Fig. 7). This is reminiscent of the differential

dependence of Ca^{2+} vs. Cd^{2+} block on specific glutamate residues in L-channels, suggesting an asymmetrical arrangement of the four negative charges in the pore (Yang et al. 1993). A T channel, with two glutamates and two aspartates at the presumed selectivity filter (Perez-Reyes et al. 1998), is clearly asymmetrical. This aspect of our model also differs from previous suggestions for Ba^{2+}–Ca^{2+} selectivity, which used symmetrical profiles, but with differences in rates of ion entry and/or exit (Almers and McCleskey 1984; Hess and Tsien 1984; Serrano et al. 2000).

Models and Mechanisms

Our model is based on the 2S3B model of Almers and McCleskey (1984), where ion–ion repulsion affects only exit, instead of Hess and Tsien (1984), where both entry and exit rates are affected. We can fit the data if ion entry is slowed by occupancy (not shown), but we prefer the idea that ion–ion repulsion primarily affects ion exit, since the rates for ion entry are close to the diffusion limit, and are only weakly voltage-dependent. That is, the barriers for ion entry mainly reflect diffusion into the mouth of the pore, not interactions with the pore. If the ion does not see an ion at the opposite binding site until it has passed the transition state for ion entry, the entry rate should be unaffected.

Is a 2S3B model inconsistent with the view that a calcium channel pore contains a single high-affinity Ca^{2+}-binding site? Perhaps there is a single, complex site within the pore that can either bind one calcium ion with high affinity, or two with low affinity. Yang et al. (1993) proposed that the four carbonyl groups move flexibly to coordinate ions as necessary. Strictly speaking, such flexibility is beyond the scope of a 2S3B model, but the idea of two preexisting sites (which cannot simultaneously bind two ions with high affinity) is not far from the contemporary view. Also note that one site is higher affinity than the other in our preferred model ($Q = 5$, Fig. 1a).

If 2S3B (and other Eyring) models are to be abandoned, it is not entirely clear what should replace them. Full-scale molecular dynamic simulations of channel permeation remain far too slow to generate I-V relationships over a range of experimental conditions comparable to those reported here, and the lack of calcium channel structure at atomic resolution would require reliance on homology models based on the quite distantly related K^+ channel family. Poisson–Nernst–Planck theory can account for an impressive number of features of calcium channel permeation (Nonner and Eisenberg 1998). We previously were unable to obtain a satisfactory quantitative description of a more limited data set for $Ca_V3.1$ using PNP (Serrano et al. 2000), but we have not yet explored more sophisticated versions of that theory (Boda et al. 2006, 2009; Nonner et al. 2000). We expect that the data set explored here, combined with data on other di- and trivalent cations (Obejero-Paz et al. 2004, 2008), will be useful to constrain and test future theoretical descriptions of calcium channel permeation. At the very least, the model presented here is a challenge to the field to present a plausible model that can provide a better description of our experimental data.

Acknowledgments This work was supported by National Institutes of Health grant NS24771 to S.W. Jones.

References

Almers W, McCleskey EW (1984) Non-selective conductance in calcium channels of frog muscle: calcium selectivity in a single-file pore. J Physiol 353:585–608

Almers W, McCleskey EW, Palade PT (1984) A non-selective cation conductance in frog muscle membrane blocked by micromolar external calcium ions. J Physiol 353:565–583

Andersen OS (1999) Graphic representation of the results of kinetic analyses [editorial]. J Gen Physiol 114:589–590

Bergling S (1999) Which model is best? Let the data decide. J Gen Physiol 114:591

Bittner KC, Hanck DA (2008) The relationship between single channel and whole cell conductance in the T-type Ca^{2+} channel $Ca_V3.1$. Biophys J 95:931–941

Boda D, Valisko M, Eisenberg B, Nonner W, Henderson D, Gillespie D (2006) The effect of protein dielectric coefficient on the ionic selectivity of a calcium channel. J Chem Phys 125:34901

Boda D, Valisko M, Henderson D, Eisenberg B, Gillespie D, Nonner W (2009) Ionic selectivity in L-type calcium channels by electrostatics and hard-core repulsion. J Gen Physiol 133:497–509

Chow CC, White JA (1996) Spontaneous action potentials due to channel fluctuations. Biophys J 71:3013–3021

Dang TX, McCleskey EW (1998) Ion channel selectivity through stepwise changes in binding affinity. J Gen Physiol 111:185–193

Gillespie DT (1977) Exact stochastic simulation of coupled chemical reactions. J Phys Chem 81:2340–2361

Hess P, Tsien RW (1984) Mechanism of ion permeation through calcium channels. Nature 309:453–456

Hodgkin AL, Huxley AF (1952) The components of membrane conductance in the giant axon of Loligo. J Physiol 116:473–496

Khan N, Gray IP, Obejero-Paz CA, Jones SW (2008) Permeation and gating in CaV3.1 (α1G) T-type calcium channels effects of Ca^{2+}, Ba^{2+}, Mg^{2+}, and Na^+. J Gen Physiol 132:223–238

Kuo CC, Hess P (1992) A functional view of the entrances of L-type Ca^{2+} channels: estimates of the size and surface potential at the pore mouths. Neuron 9:515–526

Levitt DG (1986) Interpretation of biological ion channel flux data—reaction-rate versus continuum theory. Annu Rev Biophys Biophys Chem 15:29–57

Lux HD, Carbone E, Zucker H (1990) Na^+ currents through low-voltage-activated Ca^{2+} channels of chick sensory neurones: block by external Ca^{2+} and Mg^{2+}. J Physiol 430:159–188

McCleskey EW (1999) Calcium channel permeation: a field in flux. J Gen Physiol 113:765–772

McCleskey EW, Almers W (1985) The Ca channel in skeletal muscle is a large pore. Proc Natl Acad Sci USA 82:7149–7153

Nonner W, Eisenberg B (1998) Ion permeation and glutamate residues linked by Poisson-Nernst-Planck theory in L-type calcium channels. Biophys J 75:1287–1305

Nonner W, Chen DP, Eisenberg B (1999) Progress and prospects in permeation. J Gen Physiol 113:773–782

Nonner W, Catacuzzeno L, Eisenberg B (2000) Binding and selectivity in L-type calcium channels: a mean spherical approximation. Biophys J 79:1976–1992

Obejero-Paz CA, Gray IP, Jones SW (2004) Y^{3+} block demonstrates an intracellular activation gate for the α1G T-type Ca^{2+} channel. J Gen Physiol 124:631–640

Obejero-Paz CA, Gray IP, Jones SW (2008) Ni^{2+} block of $Ca_V3.1$ (α1G) T-type calcium channels. J Gen Physiol 132:239–250

Perez-Reyes E, Cribbs LL, Daud A, Lacerda AE, Barclay J, Williamson MP, Fox M, Rees M, Lee JH (1998) Molecular characterization of a neuronal low-voltage-activated T-type calcium channel. Nature 391:896–900

Serrano JR, Dashti SR, Perez-Reyes E, Jones SW (2000) Mg^{2+} block unmasks Ca^{2+}/Ba^{2+} selectivity of α1G T-type calcium channels. Biophys J 79:3052–3062

Woodhull AM (1973) Ionic blockage of sodium channels in nerve. J Gen Physiol 61:687–708

Yamashita N, Ciani S, Hagiwara S (1990) Effects of internal Na^{+} on the Ca channel outward current in mouse neoplastic B lymphocytes. J Gen Physiol 96:559–579

Yang J, Ellinor PT, Sather WA, Zhang JF, Tsien RW (1993) Molecular determinants of Ca^{2+} selectivity and ion permeation in L-type Ca^{2+} channels. Nature 366:158–161

Yue DT, Marban E (1990) Permeation in the dihydropyridine-sensitive calcium channel. Multi-ion occupancy but no anomalous mole-fraction effect between Ba^{2+} and Ca^{2+}. J Gen Physiol 95:911–939